Supporting Information

1. Materials, reagents and instruments

$HAuCl_4$ was obtained from Anhui Zeheng Technology Co., Ltd. (China). NaOH, 4-hydroxyethylpiperazine ethanesulfonic acid (HEPES), sucrose, Tween-20, and K_2CO_3 were all purchased from Sinopharm Chemical Reagent Co., Ltd. (China). Sodium citrate and bovine serum albumin (BSA) were supplied by Anhui Zeheng Technology Co., Ltd. (China) and Sigma-Aldrich (Shanghai) Trading Co., Ltd. (China), respectively.Anti-Salmonella monoclonal antibody and anti-Staphylococcus aureus antibody were acquired from Sigma-Aldrich (Shanghai) Trading Co., Ltd. (China). Goat anti-human IgG and donkey anti-sheep antibody were provided by Beijing Yiqiao Shenzhou Biotechnology Co., Ltd. (China). SARS-CoV-2 nucleocapsid (N) protein and the corresponding monoclonal antibody (MAb-15) were procured from Fapon Biotech Inc. (China). Another anti-SARS-CoV-2 N protein antibody (clone CH-14) was sourced from Beijing Kexing Biomedical Technology Co., Ltd. (China).All human serum samples were supplied by the Affiliated Hospital of Qingdao University (China) and stored at –20 °C prior to use. Ultra-pure water was supplied by Wahaha Group Co., Ltd. (Hangzhou, China).

Mass measurements were carried out using an ESI120-4 electronic balance (Shanghai Jingke). UV-Vis absorption spectra were recorded on a UV-2450 spectrophotometer (Shimadzu). Transmission electron microscopy (TEM) images were acquired with a JEM-1400 microscope (JEOL Ltd.) operating at 120 kV.

Temperature-controlled reactions were performed in a DF-101S water bath (Zihua). Centrifugation steps were conducted with a TG16-WS centrifuge (Xiangyi) and low-temperature separations used a TGL-16 refrigerated centrifuge (Xiangyi). Sample homogenization was achieved using a DS-3510DTH ultrasonic cleaner (Shangchao). Incubation under shaking conditions was performed on a 742-312 benchtop constant temperature shaker (Shanghai Hongfa Experimental Equipment Co., Ltd.). Test strips were prepared using an HGS510 desktop film coater and separated with an HGS210 high-speed shredder (Hangzhou Feng Hang Technology Co., Ltd.). Photothermal imaging was monitored by a FOTRIC 226s infrared thermal imager (Fotric Intelligent Technology, Shanghai). Liquid handling operations were completed with pipettes (Thermo Scientific).

2. Measurement of Photothermal Conversion Efficiency

The photothermal conversion efficiencies of the Au NPs and Au NSs were systematically evaluated according to established methodology [1, 2]. Specifically, aqueous dispersions of each nanomaterial (1 mL volume) were loaded into quartz cuvettes and exposed to an 808 nm laser at a power density of 1.5 W cm^{-2}. The temperature evolution was continuously monitored using a calibrated infrared thermal camera throughout the irradiation period and subsequent cooling phase. The laser illumination was maintained until a stable equilibrium temperature was achieved, after which the laser was turned off, allowing the system to cool naturally to ambient temperature.

The photothermal conversion efficiency (η) was calculated using the following

energy balance equation[2]:

$$\eta = \frac{hS(T_{max} - T_{sur}) - Q_0}{I(1 - 10^{-A_{808}})}$$

h is the overall heat transfer coefficient, *S* denotes the surface area of the cuvette, I is the incident laser power (corresponding to 1.5 W cm^{-2}), A_{808} is the absorbance of the nanoparticle dispersion at 808 nm, T_{max} and T_{sur} are the maximum steady-state temperature and ambient temperature of the nanoparticle dispersion, respectively, Q_0 represents the heat dissipation from the solvent (measured independently using pure water under identical conditions), calculated as $hS(T_{max,water} - T_{sur,water})$.

The heat transfer parameter hS was determined from the cooling kinetics using the relation:

$$hS = \frac{mC_p}{\tau_s}$$

m is the mass of the dispersion (1 g for aqueous solutions), C_p is the specific heat capacity of water (4.2 J g^{-1} $°C^{-1}$), τ_s is the system time constant derived from the cooling phase.

The time constant τ_s was obtained by linear fitting of the cooling curve, plotted as:

$$t = -\tau_s \ln(\theta)$$

where the dimensionless driving force θ is defined as:

$$\theta = \frac{T - T_{sur}}{T_{max} - T_{sur}}$$

3. **Supporting Figures and Table**

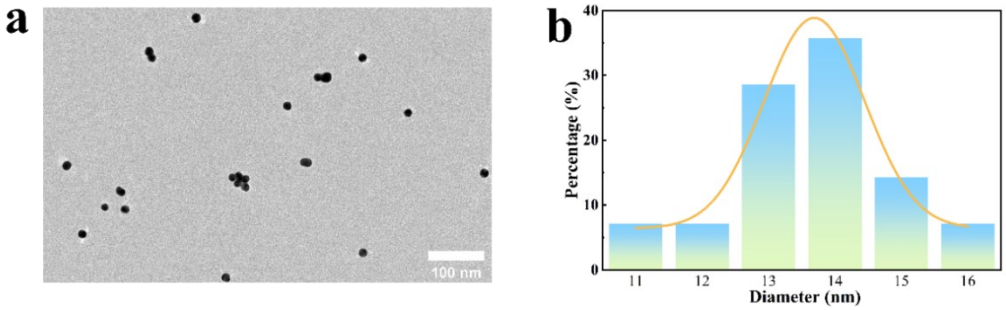

Fig. S1. (a) TEM of Au NPs. (b) Number distribution of the Au NPs size.

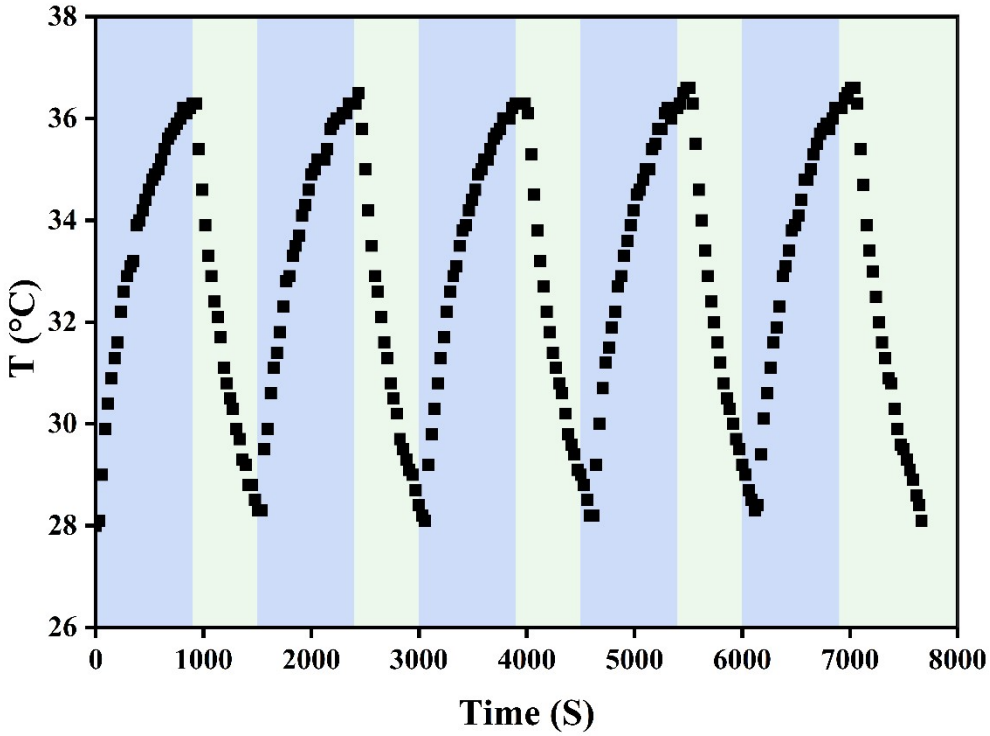

Fig. S2. Photothermal stability of Au NPs. (The power density of laser: 808 nm, 1.5 W cm^{-2}).

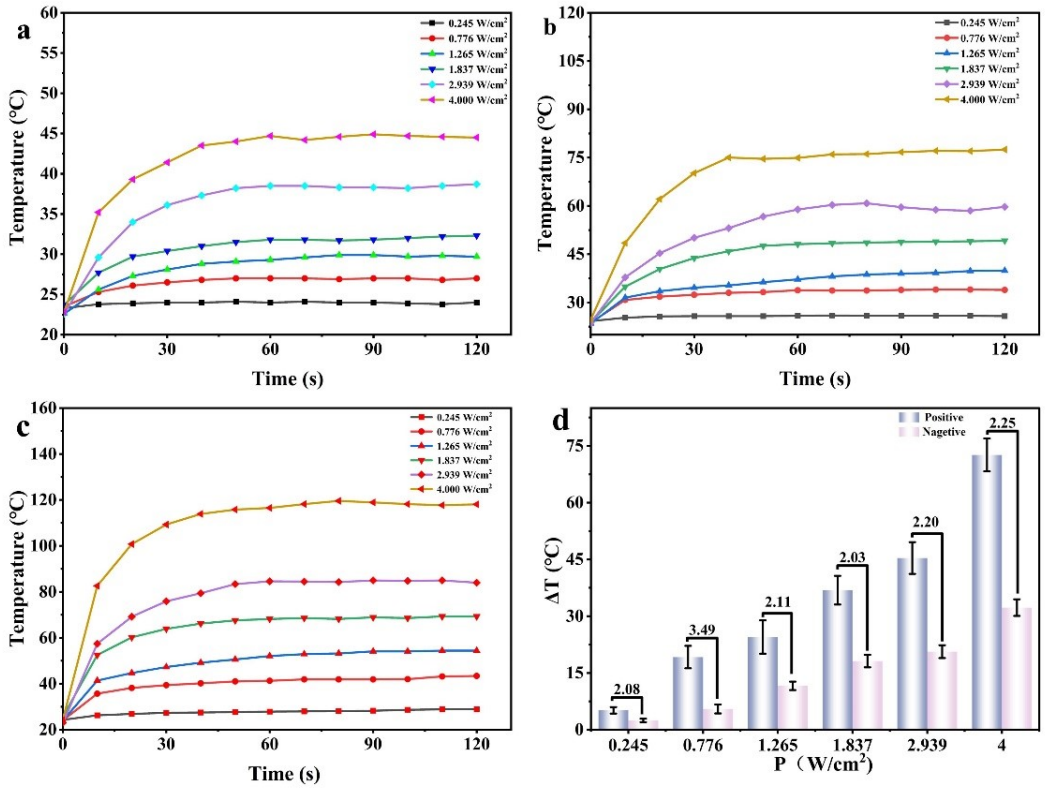

Fig. S3. Temperature elevation profiles of (a) blank, (b) negative, and (c) positive test strips under different laser power densities, and (d) corresponding signal-to-noise ratio diagram.

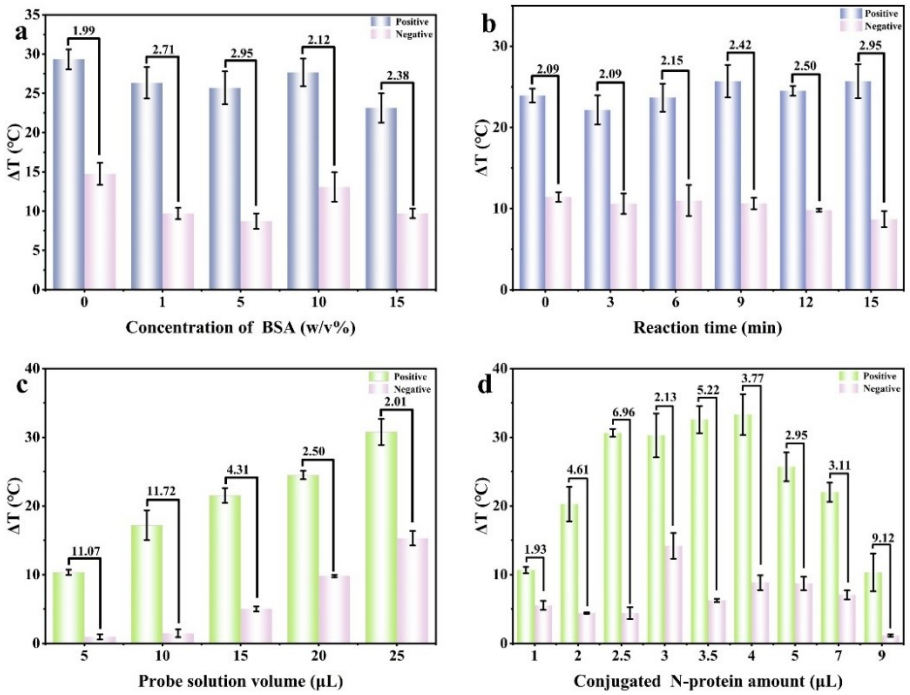

Fig. S4. (a) Optimization of blocking solution with different concentrations. (b) Optimization of reaction time. (c) Optimization of probe volume. (d) Effectiveness of different N-protein amounts.

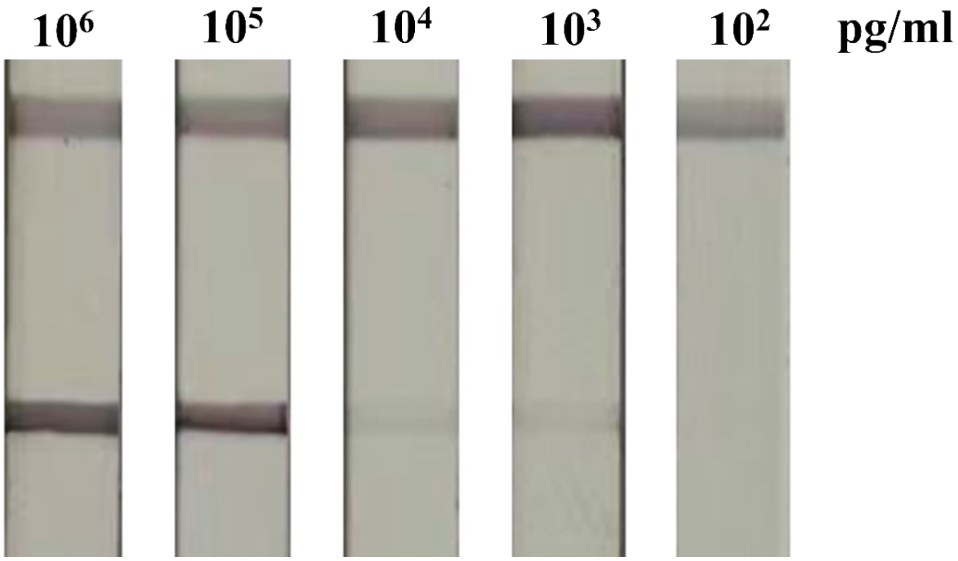

Fig. S5. Photographs of colloidal gold-based lateral flow immunoassay stripsfor antibodies at different concentrations (the asterisk indicates the visual colorimetric detection limit).

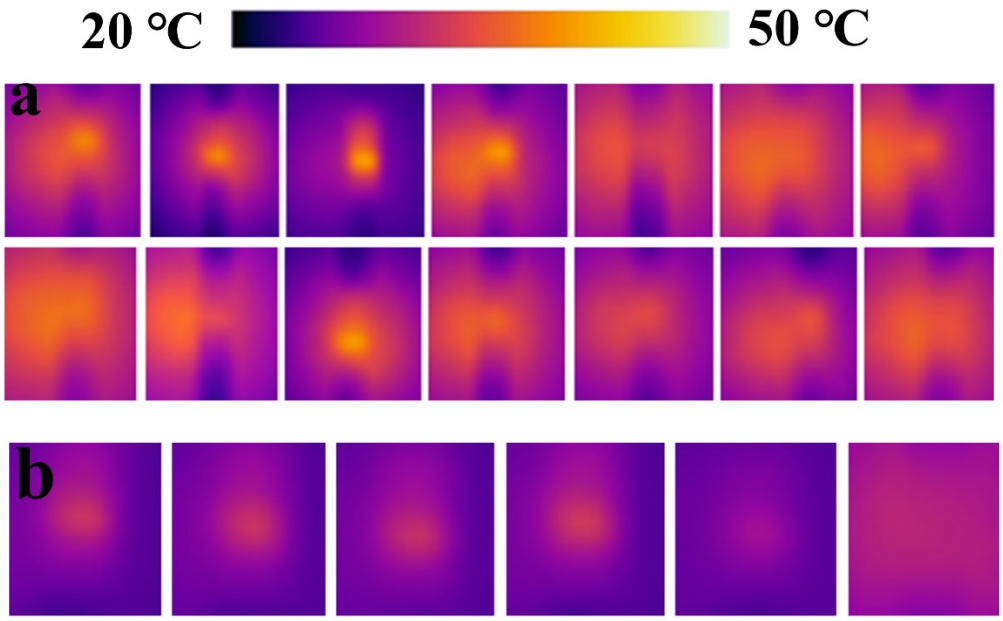

Fig. S6. Photothermal mode detection results for serum samples from the the (a): vaccinated group (n=14) and (b): unvaccinated group (n=6).

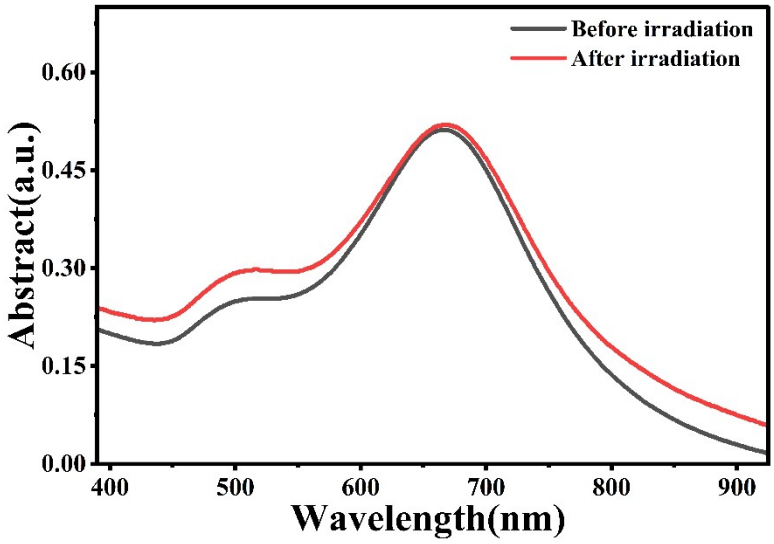

Fig. S7. UV-vis spectra of Au NSs before and after 808 nm laser irradiation at a power density of 1.265 W/cm² for 4 on/off cycles (15 min on, 15 min off per cycle).

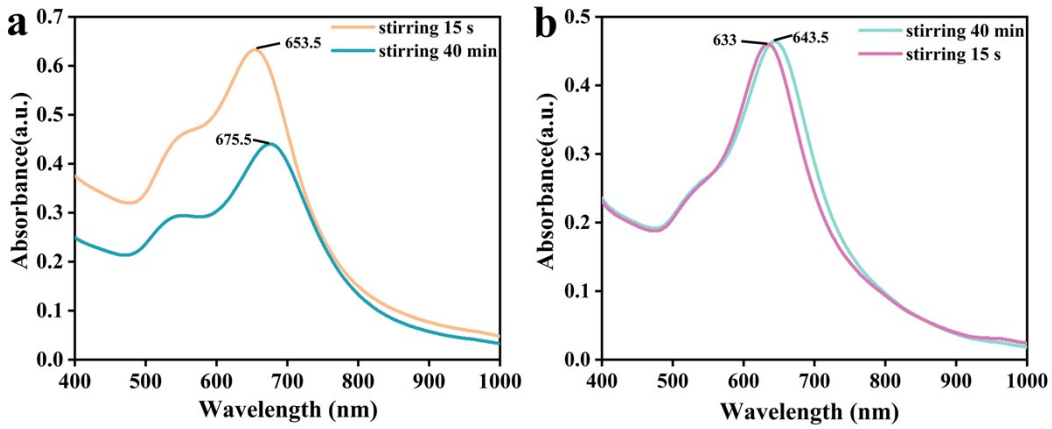

Fig. S8.(a) UV-vis absorption spectra of Au NSs synthesized with 0.25 mL of gold seeds under different stirring times (b) UV-vis absorption spectra of Au NSs synthesized with 0.1 mL of gold seeds under different stirring times

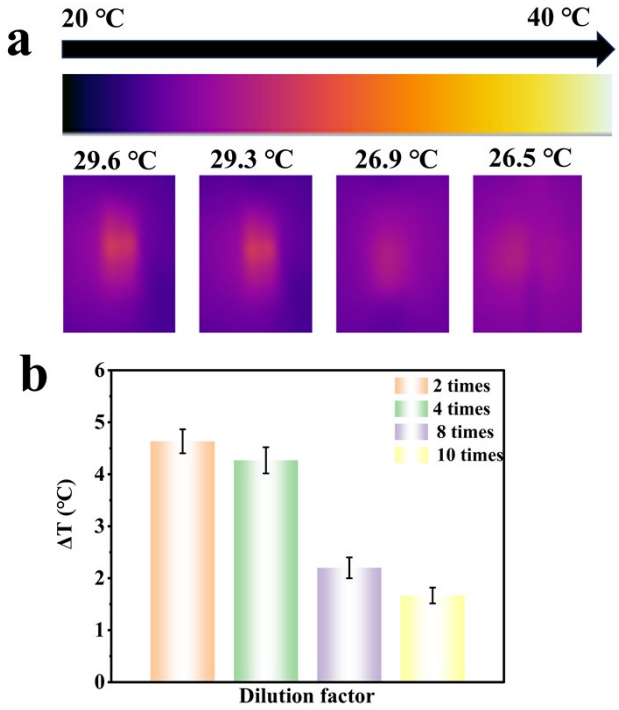

Fig. S9. Optimization of the serum dilution factor. (a) Thermal images of negative serum samples at various dilution factors (2×, 4×, 8×, and 10×). (b) Corresponding temperature changes (ΔT). Error bars represent the standard deviationof three independent measurements.

Table. S1. Summary of the analytical performances of the detection of SARS-CoV-2 antibody with different method.

Method	Label	signal	LOD	Ref

LFIA	colorimetric PDA	Color	160 ng/ml	[3]
Electrochemical	ALP	Faradaic current	1.64 ng/mL	[4]
LFIA	Au@Pt nanostars	Raman	24.91 pg/mL	[5]
ELISA	TMB enzyme	Color	9.00 ng/μL	[6]
LFIA	Colloidal gold	Color	20.66 IU/L	[7]
LFIA	Latex Microsphere	Color	48 ng/mL	[8]
LFIA	Gold-silver alloy hollow nanoshells	Color, photothermal, and SERS	20 ng/mL	[9]
LFIA	AIE 490 NP	Fluorescence	1.29 IU/mL	[10]
LFIA	Polydopamine Nanoparticles	Color	1.51 ng/mL	[11]
LFIA	Colloidal gold	Color	7.8 ng/mL	[12]
LFIA	ZnCdSe/ZnS QDs	Fluorescence	48.84 ng/mL	[13]
LFIA	Au nanostars	photothermal	107 pg/ml	This work

References

1. D. K. Roper, W. Ahn and M. Hoepfner, *The journal of physical chemistry. C, Nanomaterials and interfaces*, 2007, **111**, 3636-3641. DOI: 10.1021/jp064341w

2. D. Xi, M. Xiao, J. Cao, L. Zhao, N. Xu, S. Long, J. Fan, K. Shao, W. Sun, X. Yan and X. Peng, *ADV MATER*, 2020, **32**, e1907855. DOI: 10.1002/adma.201907855

3. H. Tong, C. Cao, M. You, S. Han, Z. Liu, Y. Xiao, W. He, C. Liu, P. Peng, Z. Xue, Y. Gong, C. Yao and F. Xu, *BIOSENS BIOELECTRON*, 2022, **213**. DOI: 10.1016/j.bios.2022.114449

4. R. Peng, Y. Pan, Z. Li, Z. Qin, J. M. Rini and X. Liu, *BIOSENS BIOELECTRON*, 2022, **197**. DOI: 10.1016/j.bios.2021.113762

5. J. Zhu, G. Guo, J. Liu, X. Li, X. Yang, M. Liu, C. Fu, J. Zeng and J. Li, *ANAL CHIM ACTA*, 2024, **1292**. DOI: 10.1016/j.aca.2024.342241
6. S. Kasetsirikul, M. Umer, N. Soda, K. R. Sreejith, M. Shiddiky and N. T. Nguyen, *ANAL YST*, 2020, **145**, 7680-7686. DOI: 10.1039/d0an01609h
7. H. Yu, H. Liu, Y. Yang and X. Guan, *ACS OMEGA*, 2022, **7**, 36254-36262. DOI: 10.1021/acsomega.2c03677
8. Z. Liang, T. Peng, X. Jiao, Y. Zhao, J. Xie, Y. Jiang, B. Meng, X. Fang, X. Yu and X. Dai, *Biosensors*, 2022, **12**, 103. DOI: 10.3390/bios12020103
9. T. Zhao, P. Liang, J. Ren, J. Zhu, X. Yang, H. Bian, J. Li, X. Cui, C. Fu, J. Xing, C. Wen and J. Zeng, *ANAL CHIM ACTA*, 2023, **1255**, 341102. DOI: 10.1016/j.aca.2023.341102
10. L. Bian, Q. Fu, Z. Gan, Z. Wu, Y. Song, Y. Xiong, F. Hu and L. Zheng, *Advanced science (Weinheim, Baden-Wurttemberg, Germany)*, 2024, **11**, e2305774. DOI: 10.3390/bios13030352
11. Z. Liu, C. Cao, H. Tong and M. You, *Biosensors*, 2023, **13**, 352. DOI: 10.3390/bios13030352
12. Z. Li, A. Wang, J. Zhou, Y. Chen, H. Liu, Y. Liu, Y. Zhang, P. Ding, X. Zhu, C. Liang, Y. Qi, E. Liu and G. Zhang, *International journal of molecular sciences*, 2022, **23**, 6225. DOI: 10.3390/ijms23116225
13. W. Deenin, N. Khongchareonporn, K. Ruxrungtham, C. Ketloy, N. Hirankarn, K. Wangkanont, S. Rengpipat, A. Yakoh and S. Chaiyo, *ANAL CHEM*, 2024, **96**, 5407-5415. DOI: 10.1021/acs.analchem.3c05144